Obstacle Avoidance Control for Two-Wheeled Drones Considering Sideslip Based on Control Barrier Functions

Keigo Mori[a], Satoshi Nakano[a], and Manabu Yamada[a]

[a]Graduate School of Engineering, Nagoya Institute of Technology; Gokiso-cho, Showa-ku, Nagoya, Aichi 466-8555, JAPAN

ARTICLE HISTORY
Compiled February 7, 2024

ABSTRACT

In this paper, we propose an obstacle avoidance control for two-wheeled drones considering sideslip based on control barrier functions. First, we derive the Lagrange equation of two-wheeled drones on a wall. Next, we propose a trajectory tracking control law for two-wheeled drones and prove that the equilibrium point of the system is almost global asymptotically stable. Then, we propose an obstacle avoidance control law for two-wheeled drones considering sideslip on the wall. Finally, We confirm the effectiveness of the proposed control law for two-wheeled drones by numerical simulations.

KEYWORDS
Drone; HyTAQs; Nonholonomic; Trajectory Tracking; Cascade Systems; Stability; ECBF-QP; Obstacle Avoidance; Sideslip

1. Introduction

Exterior wall tiles used in many buildings can be peeled off and falled because of aging. Therefore, it is necessary to inspect the exterior wall tiles every 10 years. Normally, the inspection is carried out by engineers, but the inspection depends on the experience of the engineers and involves work at high places. In fact, among the labor accidents, the number of fatal accidents in construction industries is the highest, and the number of falling is the highest. To solve such problems, it is expected that drones will conduct tapping inspections and infrared inspections without depending on experience and with less risk. By manually controlling wheeled drones, engineers can inspect without taking risks. However, manual control depends on the experience of engineers.

Therefore, in this paper, we propose an autonomous control of wheeled drones. Research on autonomous control of drones without wheels [1–3] and research on autonomous control of HyTAQs (Hybrid Terrestrial and Aerial Quadrotors) [4–6] have been conducted. Two-wheeled drones have a system with nonholonomic constraints. It is known that there is no continuous static state feedback controller that makes the origin of the system of unicycle mobile robots almost global asymptotically stable [7]. Furthermore, the attitude of two-wheeled drones is a nonlinear configuration space with a unit circle, so there is no continuous static state feedback that makes

CONTACT Keigo Mori. Email: k.mori.452@stn.nitech.ac.jp

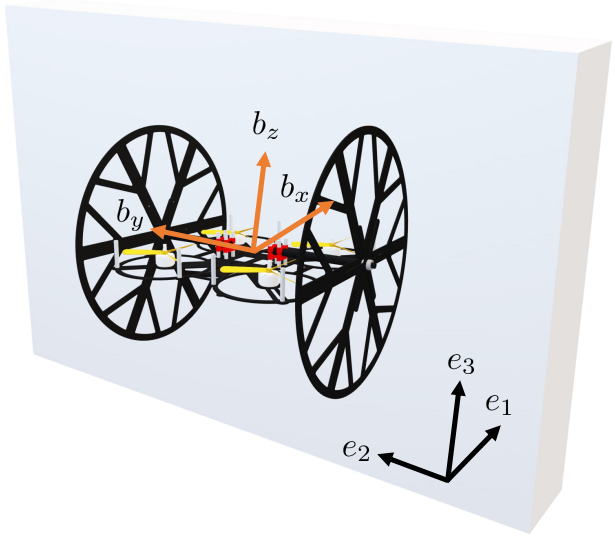

Figure 1. Two-wheeled drone moving on a wall.

the system global asymptotically stable [8]. Controllers for two-wheeled drones with nonholonomic constraints has been proposed [9] Two-wheeled drones have an additional degree of freedom because they need to consider the rotation of pitch direction in addition to the rotation in roll direction on the wall. Therefore, in this paper, we extend the attitude control, and propose the control law that includes dynamics not considered in [9]. Furthermore, since drones have a cascade structure, they are necessary to consider the interconnection term [10] to discuss stability. We prove that the origin of the system of two-wheeled drones with the control law in this paper is almost globally asymptotically stable [11].

In wall inspections, there is a risk that drones will be damaged if they collide with windows, pipes, etc. when running on the wall, so two-wheeled drones need to avoid obstacles on the wall. Control barrier functions (CBFs) have been studied in recent years to ensure the safety of systems [12–15]. For example, it has been applied to ACC (Adaptive Cruise Control) of automobiles [16,17] and obstacle avoidance for nonholonomic systems[18,19]. There are also studies on control laws using CBFs for drones to avoid obstacles [20,21]. In this paper, we use ECBF to avoid obstacles. In obstacle avoidance of two-wheeled drones on the wall, the roll is likely to become large and it is easy to slip. On the other hand, by tilting the pitch and pressing the aircraft against the wall, it is less likely to slip. Therefore, we propose a control law to avoid slipping by modifying the torque in the pitch direction using control barrier functions. Furthermore, we conduct numerical simulations using the proposed control law to verify the effectiveness of this control law.

2. Preliminaries

2.1. Two-wheeled drone model

Consider a two-wheeled drone moving on a wall illustrated in Fig. 1. We choose an inertial frame $e_i \in \mathbb{R}^3$, $i \in \{1, 2, 3\}$ and a body-fixed frame $\{b_x, b_y, b_z\}$. The origin of the body-fixed frame is the center of mass of the drone. The mass of the drone is $m \in \mathbb{R}$, acceleration of gravity is $g \in \mathbb{R}$, inertia tensor is $J \in \mathbb{R}^{3\times3}$, rotation matrix is $R \in SO(3)$, ZXY Euler angles is $\eta = [\alpha\ \beta\ \gamma]^T \in \mathbb{R}^3$, body angular velocity is $\omega^b = [\omega_1^b\ \omega_2^b\ \omega_3^b]^T \in \mathbb{R}^3$, position in the world frame is $p = [x\ y\ z]^T \in \mathbb{R}^3$, body velocity is $v^b = [v_1^b\ v_2^b\ v_3^b]^T \in \mathbb{R}^3$, thrust is $F^b = [0\ 0\ f] \in \mathbb{R}^3$, body torque is $\tau^b \in \mathbb{R}^3$.

The kinematics of the translational motion is given by

$$\dot{p} = Rv^b = \begin{bmatrix} 0 \\ -\frac{v_3^b \sin\beta}{\cos\gamma} \\ \frac{v_3^b \cos\beta}{\cos\gamma} \end{bmatrix} = \frac{1}{\cos\gamma} R_2(\beta)(v_3^b e_3) \tag{1}$$

where

$$\begin{aligned} R &= \begin{bmatrix} r_{11} & r_{12} & r_{13} \\ r_{21} & r_{22} & r_{23} \\ r_{31} & r_{32} & r_{33} \end{bmatrix} \\ &= \begin{bmatrix} \cos\gamma & 0 & \sin\gamma \\ \sin\beta\sin\gamma & \cos\beta & -\sin\beta\cos\gamma \\ -\cos\beta\sin\gamma & \sin\beta & \cos\beta\cos\gamma \end{bmatrix} \end{aligned}$$

$$R_2(\beta) = \begin{bmatrix} 1 & 0 & 0 \\ 0 & \cos\beta & -\sin\beta \\ 0 & \sin\beta & \cos\beta \end{bmatrix}.$$

The kinematics of the rotational motion in the ZXY Euler angles representation is given by

$$\dot{\eta} = \Phi(\eta)\omega^b \tag{2}$$

where

$$\Phi(\eta) = \begin{bmatrix} \frac{\sin\gamma}{\cos\beta} & 0 & \frac{\cos\gamma}{\cos\beta} \\ \cos\gamma & 0 & -\sin\gamma \\ \frac{\sin\beta\sin\gamma}{\cos\beta} & 1 & \frac{\sin\beta\cos\gamma}{\cos\beta} \end{bmatrix}.$$

The inverse of $\Phi(\eta)$ is $\Psi = \Phi^{-1}$, which is given by

$$\Psi(\eta) = \begin{bmatrix} \cos\beta\sin\gamma & \cos\gamma & 0 \\ -\sin\beta & 0 & 1 \\ \cos\beta\cos\gamma & -\sin\gamma & 0 \end{bmatrix}.$$

The dynamics of the translational motion is given by

$$m\ddot{p} + mge_3 + \lambda_1 A^T + \lambda_2 e_1 = Rfe_3. \tag{3}$$

The dynamics of the rotational motion [22] is given by

$$M(\eta)\ddot{\eta} + C(\eta, \dot{\eta})\dot{\eta} = \Psi(\eta)^T \tau^b - \lambda_3 e_1. \tag{4}$$

2.2. Exponential control barrier functions(ECBF)

CBF can be applied when the derivative of $h(x)$ is one. We relax this relative degree condition and assume that $h(x)$ has a higher relative degree $r \geq 1$, i.e., it satisfies the following equation,

$$h^{(r)}(x, u) = L_f^r h(x) + L_g L_f^{r-1} h(x) u.$$

Here, $L_g L_f^{r-1} h(x) \neq 0$ and $L_g L_f^2 h(x) = \cdots L_g L_f^{r-2} h(x) = 0$, $\forall x \in D$ We further define the following,

$$\eta_b(x) \coloneqq \begin{bmatrix} h(x) \\ \dot{h}(x) \\ \ddot{h}(x) \\ \vdots \\ h^{(r-1)}(x) \end{bmatrix} = \begin{bmatrix} h(x) \\ L_f h(x) \\ L_f^2 h(x) \\ \vdots \\ L_f^{r-1} h(x) \end{bmatrix}.$$

We assume that there exists a control input $u \in U_\mu \subset \mathbb{R}$ for $\mu \in \mathbb{R}$ such that $L_f^r h(x) + L_g L_f^{r-1} h(x) u = \mu$. Then, the dynamics of $h(x)$ can be described as the following linear system,

$$\begin{aligned} \dot{\eta}_b(x) &= F\eta_b(x) + G\mu, \\ h(x) &= C\eta_b(x) \end{aligned}$$

where

$$F = \begin{bmatrix} 0 & 1 & 0 & \cdots & 0 \\ 0 & 0 & 1 & \cdots & 0 \\ \vdots & \vdots & \vdots & \ddots & \vdots \\ 0 & 0 & 0 & \cdots & 1 \\ 0 & 0 & 0 & \cdots & 0 \end{bmatrix}, G = \begin{bmatrix} 0 \\ 0 \\ \vdots \\ 0 \\ 1 \end{bmatrix},$$
$$C = [1\ 0\ \cdots\ 0].$$

If we choose the state feedback $\mu = -K_\alpha \eta_b(x)$, then $h(x(t)) = Ce^{(F - GK_\alpha)t}\eta_b(x_0)$. Furthermore, if $\mu \geq -K_\alpha \eta_b(x)$, then $h(x(t)) \geq Ce^{(F-GK_\alpha)t}\eta_b(x_0)$ by comparison lemma.

Definition 2.1. Given a set $C \subset D \subset \mathbb{R}$, a function $h : D \to \mathbb{R}$ that is r times continuously differentiable is an exponential control barrier function(ECBF) if there

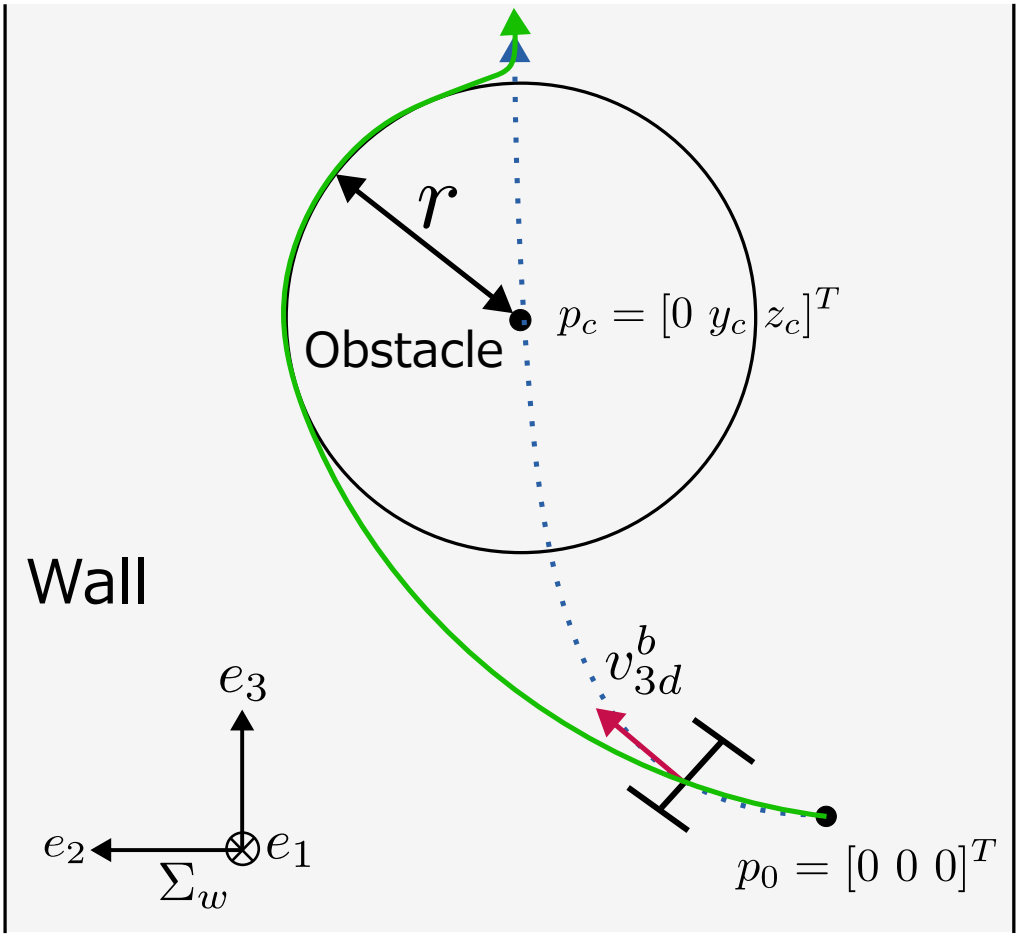

Figure 2. Outline drawing of obstacle avoidance.

exists a column vector $K_\alpha \in \mathbb{R}^r$ that satisfies the following equation for all $x \in D$,

$$\sup_{u \in U}[L_f^r h(x) + L_g L_f^{r-1} h(x) u] \geq -K_\alpha \eta_b(x).$$

Here, $\forall x \in \mathrm{Int}(C)$, $h(x(t)) \geq Ce^{(F - GK_\alpha)t}\eta_b(x_0)$ whenever $h(x_0) \geq 0$.

3. Control design

3.1. Problem settings and program formulation

Consider a two-wheeled drone moving on a wall with a circular obstacle of a center $p_c = [0, y_c, z_c]^T$ and a radius $r \in \mathbb{R}$. We show the outline drawing of the control law of this paper in Fig. 2. The blue dotted line is the image of the target trajectory, and the green solid line is the image of the trajectory when the obstacle avoidance control is used. When the target trajectory is inside the obstacle, it is necessary to avoid the obstacle. However, if the drone tries to avoid the obstacle by rolling on the

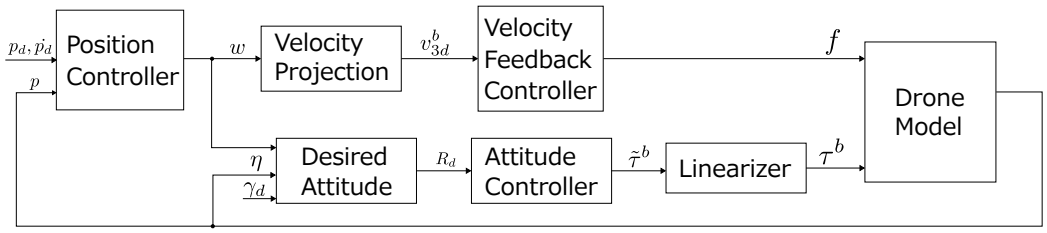

Figure 3. Block diagram of the proposed control structure.

wall, the gravity component in the lateral direction becomes large, and there is a risk of slipping. Therefore, the control objective of this paper is to avoid obstacles without slipping. The condition for not slipping is expressed by the following equation,

$$\|\lambda_1 A^T\| \leq \mu \|\lambda_2 e_1\|. \tag{5}$$

where coefficient of static friction is $\mu \in \mathbb{R}$, slipping force is $\|\lambda_1 A^T\|$, and pushing force to the wall is $\|\lambda_2 e_1\|$. $A^T = [0\ r_{22}\ r_{32}]^T$ gives $\|A^T\| = 1$ and since $\|\lambda_2 e_1\|$ is pushing force, $\lambda_2 \geq 0$. Therefore, we can transform the equation (5) as follows,

$$\|\lambda_1\| \leq \mu \lambda_2. \tag{6}$$

Hence, the control objective of this paper is to design the input f, τ^b that satisfies the condition (6) and the following equation,

$$\begin{cases} \lim\limits_{t\to\infty} \|p - p_d\| = 0 & \text{if } \|p_d - p_c\| > r \\ \|p - p_c\| \geq r & \text{otherwise.} \end{cases}$$

The control structure of this paper is shown in Fig. 3. We design the control law of translational motion based on kinematics. Therefore, we design the velocity feedback control law for velocity projection, and by using this, we finally get the thrust. Furthermore, we design the control law of rotational motion based on linearized dynamics.

3.2. Linearlization of rotational dynamics and pitch controller

We define a new virtual input $\tilde{\tau}^b \in \mathbb{R}^3$ as follows,

$$\tau^b = J\Psi(\eta)\tilde{\tau}^b + \left(\Psi(\eta)^T\right)^{-1} C(\eta, \dot{\eta})\dot{\eta} + \lambda_3 e_1.$$

Then, the rotational dynamics (4) can be linearized as follows,

$$\ddot{\eta} = \tilde{\tau}^b. \tag{7}$$

When running on the wall, it is important for two-wheeled drones to push the drone against the wall. This is because the stability of the drone against sideslip or side wind is increased and the grip is improved. By (7), the linearized dynamics of the pitch

direction is given by the following equation,

$$\ddot{\gamma} = \tilde{\tau}_{\gamma}^{b}. \tag{8}$$

We design the pitch controller as follows,

$$\tilde{\tau}_{\gamma}^{b} = -k_{p_{\gamma}}(\gamma - \gamma_d) - k_{d_{\gamma}}(\dot{\gamma} - \dot{\gamma}_d) \tag{9}$$

where $k_{p_{\gamma}}, k_{d_{\gamma}} > 0$.

3.3. Translational controller

In this paper, we propose a trajectory tracking control law for two-wheeled drones based on the control law for unicycle mobile robots [9]. Suppose that the position y, z of the drone is $X = [y\ z]^T \in \mathbb{R}^2$, the target position of y, z is $X_d = [y_d\ z_d]^T \in \mathbb{R}^2$, the position error of y, z is $\tilde{X} = [y - y_d\ z - z_d]^T = X - X_d \in \mathbb{R}^2$, and the positive definite matrix $K_p > 0$. The desired velocity $w = [w_y\ w_z] \in \mathbb{R}^2$ is designed by the following translational controller,

$$w = \cos\gamma_d(-K_p\tilde{X} + \dot{X}_d). \tag{10}$$

Considering the nonholonomic constraint $v_2^b = 0$, the desired velocity w is transformed into the projection velocity by the following equation,

$$v_{3d}^{b} = w^T \left(E^T R_2(\beta) E\right)\left(E^T e_3\right) \tag{11}$$

where $E = [e_2\ e_3] \in \mathbb{R}^{3\times 2}$.

3.4. Roll controller

The linearized dynamics of the roll is given by the following equation,

$$\ddot{\beta} = \tilde{\tau}_{\beta}^{b} \tag{12}$$

Then, the roll controller for (12) is given by the following equation,

$$\begin{cases} \tilde{\tau}_{\beta}^{b} & = -k_{\beta}(\dot{\beta} - r_{\beta}) + \dot{r}_{\beta} \\ r_{\beta} & = r_{\beta_d} - k_R(\mathrm{sk}(\tilde{R}))^{\vee} \end{cases} \tag{13}$$

where $k_{\beta} > 0$ and

$$\begin{cases} \tilde{R} & = R_d^T E^T R_2(\beta) E \\ R_d & = \left[(-1)^{\wedge}\frac{w}{\|w\|}\ \ \frac{w}{\|w\|}\right] \\ r_{\beta_d} & = (R_d^T \dot{R}_d)^{\vee}. \end{cases} \tag{14}$$

3.5. Translational dynamics and velocity feedback

We design the controller to obtain the thrust from the velocity projection v_{3d}^b obtained by the translational controller. (3) and (1) give the following equation,

$$f = m(f_1 \dot{v}_3^b + f_2 + f_3)$$

where

$$\begin{cases} f_1 &= 1 - \frac{r_{13}(r_{32}r_{21} - r_{22}r_{31})}{r_{11}(r_{32}r_{23} - r_{22}r_{33})} \\ f_2 &= \frac{v_3^b \omega_2^b (r_{32}r_{21} - r_{22}r_{31} - r_{11}) - g r_{11} r_{22} + \omega_2^b r_{13} v_1^b}{r_{11}(r_{32}r_{23} - r_{22}r_{33})} \\ f_3 &= v_1^b \omega_2^b. \end{cases}$$

Therefore, the velocity feedback control law $\dot{v}_3^b = -k_3(v_3^b - v_{3d}^b) + \dot{v}_{3d}^b$ is applied by the positive constant $k_3 > 0$. Then, the thrust is given by the following equation,

$$f = m\left(f_1\left(-k_3\left(v_3^b - v_{3d}^b\right) + \dot{v}_{3d}^b\right) + f_2 + f_3\right).$$

We prove the equilibrium point of the system with the controller is almost globally asymptotically stable. We investigate the stability of the origin of the system in the rotational motion and the translational motion, respectively, and then discuss the stability of the entire system by combining the rotational motion and the translational motion. First, from (8) and (9), the linearized dynamics of the pitch direction is given by the following equation,

$$\ddot{\gamma} - \ddot{\gamma}_d = -k_{p_\gamma}(\gamma - \gamma_d) - k_{d_\gamma}(\dot{\gamma} - \dot{\gamma}_d) \tag{15}$$

(15) can be rewritten as follows,

$$\ddot{\gamma}_e = -k_{p_\gamma}\gamma_e - k_{d_\gamma}\dot{\gamma}_e \tag{16}$$

where $\gamma_e = \gamma - \gamma_d$. Therefore, (16) is rewritten as follows,

$$\frac{d}{dt}\begin{bmatrix}\gamma_e \\ \dot{\gamma}_e\end{bmatrix} = \begin{bmatrix}0 & 1 \\ -k_{p_\gamma} & -k_{d_\gamma}\end{bmatrix}\begin{bmatrix}\gamma_e \\ \dot{\gamma}_e\end{bmatrix}. \tag{17}$$

Therefore, the eigenvalue is negative, so the origin of the system (17) is global asymptotically stable. From (12) and (13), the linearized dynamics of the roll direction is given by the following equation,

$$\ddot{\beta} = -k_\beta(\dot{\beta} - r_\beta) + \dot{r}_\beta. \tag{18}$$

(18) can be rewritten as follows,

$$\ddot{\beta}_e = -k_\beta \dot{\beta}_e \tag{19}$$

where $\dot{\beta}_e = \dot{\beta} - r_\beta$. Therefore, the system (19) is asymptotically stable. (18) can be rewritten as follows,

$$\ddot{\beta} = \Delta_1 + \dot{r}_\beta \tag{20}$$

where $\Delta_1 = -k_\beta(\dot{\beta} - r_\beta)$. Furthermore, by integrating both sides of (20), we get the following equation,

$$\dot{\beta} = \int \Delta_1 dt + r_\beta = \Delta_1' + r_\beta. \tag{21}$$

By writing (21) as $SO(2)$, we get the following equation,

$$\dot{R} = R\hat{r}_\beta + \Delta_1''. \tag{22}$$

Furthermore, (22) can be rewritten as follows,

$$\dot{\tilde{R}} = \tilde{R}\hat{\tilde{r}}_\beta + \Delta_1''' \tag{23}$$

where $\tilde{r}_\beta = r_\beta - r_{\beta_d}$. Next, we consider the following equation without the term Δ_1''' in (23),

$$\dot{\tilde{R}} = \tilde{R}\hat{\tilde{r}}_\beta. \tag{24}$$

From [9], $\tilde{R} = I$ and $\tilde{R} = -I$ are the only equilibrium points of the system (24), and $\tilde{R}_e = -I$ is an unstable equilibrium point, and it almost globally asymptotically converges to $\tilde{R} = I$. The main result about the direction of rotation is as follows.

Theorem 3.1. *The equilibrium point of the system* (23) $\tilde{R}_e = -I$ *is unstable, and the desired equilibrium point* $\tilde{R}_e = I$ *is almost globally asymptotically stable if the controller* (13) *is designed to the rotational error dynamics* (23).

Proof. When the controller (13) is applied to the system (12), the origin of the system (12) is almost global asymptotically stable, so $\lim_{t\to\infty} \dot{\beta} = r_\beta$ holds. Therefore, $\lim_{t\to\infty} \Delta_1' = 0$ holds. Furthermore, when the controller (13) is applied to (24), the equilibrium point $\tilde{R}_e = -I$ is unstable, and the desired equilibrium point $\tilde{R}_e = I$ is almost global asymptotically stable. Hence, similar to the system (23), the equilibrium point $\tilde{R}_e = -I$ is unstable, and the desired equilibrium point $\tilde{R}_e = I$ is almost globally asymptotically stable. □

Therefore, the origin of (17) and (23) are almost global asymptotically stable if the controller (9) and (13) are applied to the system (17) and (23) respectively.

Next, we consider the stability of the translational motion. From (1), the yz kinematics of the translational motion is given by the following equation,

$$\begin{aligned}\dot{X} &= \frac{1}{\cos\gamma}(v_{3d}^b - \tilde{v}_3^b)(E^T R_2(\beta)E)(E^T e_3) \\ &= \frac{v_{3d}^b}{\cos\gamma_d}(E^T R_2(\beta)E)(E^T e_3) + \Delta_2 + \Delta_3\end{aligned} \tag{25}$$

where $\tilde{v}_3^b = v_{3d}^b - v_3^b$ and

$$\Delta_2 = -\frac{v_{3d}^b}{\cos\gamma_d}(E^T R_2(\beta)E)(E^T e_3) + \frac{v_{3d}^b}{\cos\gamma}(E^T R_2(\beta)E)(E^T e_3)$$

$$\Delta_3 = -\frac{\tilde{v}_3^b}{\cos\gamma}(E^T R_2(\beta)E)(E^T e_3).$$

Here, we consider the following equation without the term Δ_2 and Δ_3 in (25),

$$\dot{X} = \frac{v_{3d}^b}{\cos\gamma_d}(E^T R_2(\beta)E)(E^T e_3). \tag{26}$$

Here, (26) can be rewritten as follows,

$$\dot{X} = \frac{1}{\cos\gamma_d}\frac{v_{3d}^b R_d(E^T e_3)}{(E^T e_3)^T\tilde{R}(E^T e_3)} + \frac{1}{\cos\gamma_d}\frac{v_{3d}^b}{(E^T e_3)^T\tilde{R}(E^T e_3)} \left((E^T e_3)^T\tilde{R}(E^T e_3)(E^T R_2(\beta)E) - R_d(E^T e_3)\right).$$

From (11) and the second equation of (14), we get the following equation,

$$\dot{\tilde{X}} = \frac{1}{\cos\gamma_d}w + \frac{1}{\cos\gamma_d}\|w\| \left(\left(\left(E^T e_3\right)^T\tilde{R}\left(E^T e_3\right)\right)R_d\tilde{R}\left(E^T e_3\right) - R_d\left(E^T e_3\right)\right). - \dot{X}_d. \tag{27}$$

Therefore, the error system containing the translational kinematics, dynamics, velocity feedback, and the velocity projection was derived. Then, (27) is given by the following equation,

$$\dot{\tilde{X}} = -K_p\tilde{X} + \|w\| \left(\left(\left(E^T e_3\right)^T\tilde{R}\left(E^T e_3\right)\right)R_d\tilde{R}\left(E^T e_3\right) - R_d\left(E^T e_3\right)\right).$$

Hence, the following theorem is obtained from Proposition 3 of [9].

Theorem 3.2. *We assume that the target trajectory $X_d = [y_d\ z_d]^T \in \mathbb{R}^2$ satisfies the following assumption,*

$$\|\dot{X}_d\| \leq \sigma.$$

where $\sigma \in \mathbb{R}$ is a positive constant. Consider the closed system (26) *with the controller* (10)*. Then, the trajectory of the closed-loop dynamics does not escape in finite time.*

Hence, the main theorem of the stability in this paper is obtained as follows.

Theorem 3.3. *Consider the closed-loop system of the kinematics* (1), (2), *and the dynamics* (3), (4) *of the two-wheeled drones with the controller* (9), (10), *and* (13). *Then, the equilibrium points* $\tilde{p} = 0$ *and* $\tilde{R} = I$ *are almost global asymptotically stable.*

4. Control design using control barrier functions

In this chapter, we design a control barrier function (CBF) to avoid obstacles considering sideslipping.

4.1. Control design of ECBF-QP for obstacle avoidance

We consider the control barrier function as follows,

$$h_{\text{obst}} = (y - y_c)^2 + (z - z_c)^2 - r^2.$$

We consider the linearized roll torque $\tilde{\tau}_\beta^b$ as an input. Therefore, $\dddot{h}_{\text{obst}} + \alpha_1 h_{\text{obst}} + \alpha_2 \dot{h}_{\text{obst}} + \alpha_3 \ddot{h}_{\text{obst}} \geq 0$ can be written as follows,

$$f_x + g_x \tilde{\tau}_\beta^b \leq 0$$

where f_x, g_x can be obtained by Symbolic Math Toolbox in MATLAB, especially g_x is as follows,

$$\begin{aligned} g_x = 2\left((z_c - z)\sin\beta + (y_c - y)\cos\beta\right) \\ \times(-\cos\beta\dot{z} + \sin\beta\dot{y}). \end{aligned}$$

Hence, ECBF-QP for obstacle avoidance is obtained as follows,

$$\begin{cases} \tilde{\tau}_{\text{obst}}^b = \underset{\tilde{\tau}_{\text{obst}}^b \in \mathbb{R}}{\arg\min} \|\tilde{\tau}_{\text{obst}}^b - \tilde{\tau}_0^b\|^2 \\ \text{s.t.} \quad f_x + g_x \tilde{\tau}_\beta^b \leq 0. \end{cases}$$

4.2. Control design of ECBF-QP for sideslip

When avoiding obstacles, two-wheeled drones need to roll, so sideslip is likely to occur. For HyTAQs, there is research on considering sideslipping during ground running [23]. In this chapter, we design a control barrier function to avoid sideslip in addition to the control barrier function for obstacle avoidance and consider the linearized pitch toqrue $\tilde{\tau}_\gamma^b$ as an input.

Condition not to sideslip can be written as follows,

$$f_{\text{slip}} \leq \mu N \tag{28}$$

where f_{slip} is the force to make the drone sideslip, N is the force to push the drone against the wall, and μ is the coefficient of static friction. The force to make the drone sideslip is $\|\lambda_1 A^T\|$, and the force to push the drone against the wall is $\|\lambda_2 e_1\|$, so (28)

can be written as follows,

$$\|\lambda_1 A^T\| \leq \mu \|\lambda_2 e_1\|. \tag{29}$$

λ_1 can take both positive and negative values, but $\lambda_2 \geq 0$, and $\|A^T\| = 1$ and $\|e_1\| = 1$, so (29) can be written as follows,

$$\|\lambda_1\| \leq \mu \lambda_2. \tag{30}$$

The inequality (30) is an inequality containing absolute values, so we consider the conditions by dividing the cases.

If $\lambda_1 \geq 0$, (30) can be written as follows,

$$mg \sin\beta + f\mu \sin\gamma - m \cos\beta \dot{z}\dot{\beta} + m \sin\beta \dot{y}\dot{\beta} \geq 0.$$

Therefore, the control barrier function h_{slip_1} can be defined as follows,

$$\begin{aligned} h_{\text{slip}_1} \coloneqq & mg \sin\beta + f\mu \sin\gamma \\ & -m \cos\beta \dot{z}\dot{\beta} + m \sin\beta \dot{y}\dot{\beta}. \end{aligned} \tag{31}$$

(31) is a function of $\tilde{\tau}_\gamma^b$ in the second order, so the relative degree is 2. Therefore, $\ddot{h}_{\text{slip}_1} + \alpha_4 \dot{h}_{\text{slip}_1} + \alpha_5 \dot{h}_{\text{slip}_1} \geq 0$ can be written as follows,

$$f_x + g_x \tilde{\tau}_\gamma^b \leq 0$$

where f_x, g_x can be obtained by Symbolic Math Toolbox in MATLAB, especially g_x is as follows,

$$g_x = -\mu \cos\gamma f.$$

If $\lambda_1 < 0$, the control barrier function h_{slip_2} can be defined as follows similar to $\lambda_1 \geq 0$,

$$\begin{aligned} h_{\text{slip}_2} \coloneqq & f\mu \sin\gamma - mg \sin\beta \\ & +m \cos\beta \dot{z}\dot{\beta} - m \sin\beta \dot{y}\dot{\beta}. \end{aligned}$$

Therefore, $\ddot{h}_{\text{slip}_2} + \alpha_4 \dot{h}_{\text{slip}_2} + \alpha_5 \dot{h}_{\text{slip}_2} \geq 0$ can be written as follows,

$$f_x + g_x \tilde{\tau}_\gamma^b \leq 0$$

where f_x, g_x can be obtained by Symbolic Math Toolbox in MATLAB, especially g_x is as follows,

$$g_x = -\mu \cos\gamma f.$$

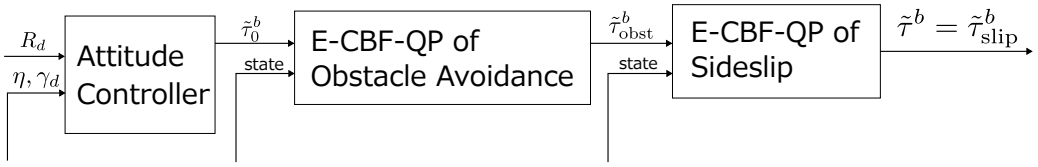

Figure 4. Control structure of ECBF-QP.

Hence, ECBF-QP for sideslip is obtained as follows,

$$\begin{cases} \tilde{\tau}_{\text{slip}}^b = \underset{\tilde{\tau}_{\text{slip}}^b \in \mathbb{R}}{\arg\min} \|\tilde{\tau}_{\text{slip}}^b - \tilde{\tau}_{\text{obst}}^b\|^2 \\ \text{s.t.} \quad f_x + g_x \tilde{\tau}_\gamma^b \leq 0. \end{cases}$$

The control structure of the ECBF-QP combined with obstacle avoidance and sideslip is shown in Fig. 4. The constraint equation of ECBF-QP for obstacle avoidance contains $\tilde{\tau}_\beta^b$, but doesn't contain $\tilde{\tau}_\gamma^b$. On the other hand, the constraint equation of ECBF-QP for sideslip contain both $\tilde{\tau}_\beta^b$ and $\tilde{\tau}_\gamma^b$. Therefore, the linearized roll torque $\tilde{\tau}_\beta^b$ is modified by the ECBF-QP for obstacle avoidance, and then, the linearized pitch torque $\tilde{\tau}_\gamma^b$ is modified by the ECBF-QP for sideslip.

5. Simulation condition and results

In this chapter, we verify that the control objectives are achieved by simulation of the control design in this paper. We consider $m = 0.938\text{kg}$, $J = \text{diag}[0.00933\ 0.00285\ 0.01130]\text{kg}\,\text{m}^2$, $g = 9.81\text{m/s}^2$ as the physical parameters of the two-wheeled drone. We also consider $k_3 = 10$ as the velocity feedback gain, $K_p = \text{diag}([0.5, 0.5, 0.5])$ as the position controller, $k_R = 4$, $k_\beta = 2$, $k_{p_\gamma} = 5$, $k_{d_\gamma} = 5$ as the attitude controller and $[y_c\ z_c] = [-0.2\ 1.0]\text{m}$, $r = 0.5\text{m}$, $\alpha_1 = 0.4$, $\alpha_2 = 0.3$, $\alpha_3 = 0.3$ as the parameters of the ECBF-QP for obstacle avoidance, and $\mu = 0.5$, $\alpha_4 = 20$, $\alpha_5 = 10$ as the parameters of the ECBF-QP for avoiding sideslip. Furthermore, the initial values are $p_0 = [0\ 0\ 0]^T\text{m}$, $\dot{p}_0 = [0\ 0\ 0]^T\text{m/s}$, $\eta_0 = [0\ 0\ \frac{5\pi}{180}]^T\text{rad}$, $\dot{\eta}_0 = [0\ 0\ 0]^T\text{rad/s}$, the target value is $\gamma_d = \frac{15\pi}{180}\text{rad}$, and the target trajectory on the wall p_d is given by the following equation,

$$p_d = \begin{bmatrix} 0 \\ 0.2\sin\frac{15\pi}{180}t\ (0 \leq t < 6), \quad 0.2\ (6 \leq t) \\ 0.2t \end{bmatrix}.$$

We show the simulation results of the position, attitude, thrust, and torque in Fig. 5, Fig. 6, Fig. 7, Fig. 8, respectively. We also show the animation of the simulation result in Fig. 9 and the trajectory on the wall in Fig. 10. From Fig. 5, Fig. 10. We can see that the two-wheeled drone avoids the obstacle and follows the target trajectory. Furthermore, we show the control barrier functions for obstacle avoidance and sideslip in Fig. 11, Fig. 12, respectively. The control barrier function for sideslip is defined by

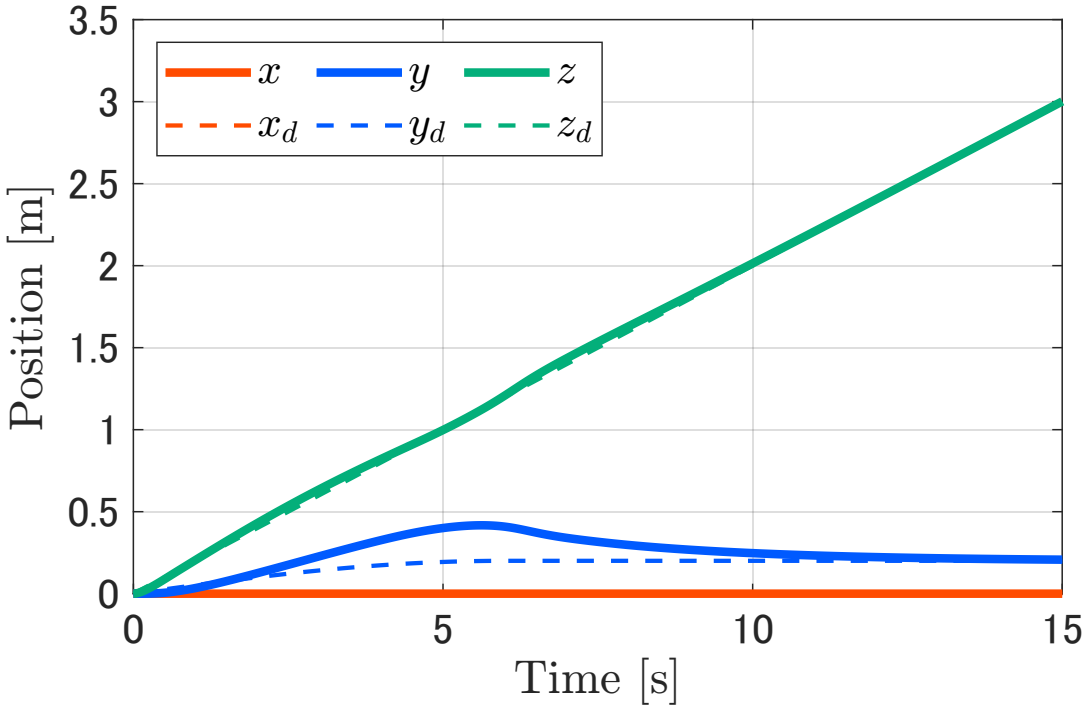

Figure 5. Simulation result of position.

the following equation,

$$h_{\text{slip}} = \begin{cases} h_{\text{slip}_1} & (\lambda_1 \geq 0), \\ h_{\text{slip}_2} & (\lambda_1 < 0). \end{cases}$$

From Fig. 11, we can see that $h_{\text{obst}} \geq 0$, and from Fig. 12, we can see that $h_{\text{slip}} \geq 0$. Therefore, the two-wheeled drone satisfies the constraints of obstacle avoidance and sideslip.

6. Conclusion

In this paper, we proposed an obstacle avoidance control for two-wheeled drones considering sideslip based on control barrier functions. First, we derived the ZXY Euler angle-based Lagrange equation of two-wheeled drones on the wall.

Next, we extended [9] and designed a control law for trajectory tracking of a wheeled drone on the wall, and proved that the origin of the system is almost globally asymptotically stable.

Furthermore, we designed ECBF-QP for obstacle avoidance and sideslip using control barrier functions, and combined them.

Finally, we confirmed the effectiveness of the proposed control law for two-wheeled drones by numerical simulations.

As a future work, we will compare the $SE(2)$-based control law for two-wheeled drones in [24] and the trajectory tracking control law in this paper, and consider the solvability conditions of CBF-QP.

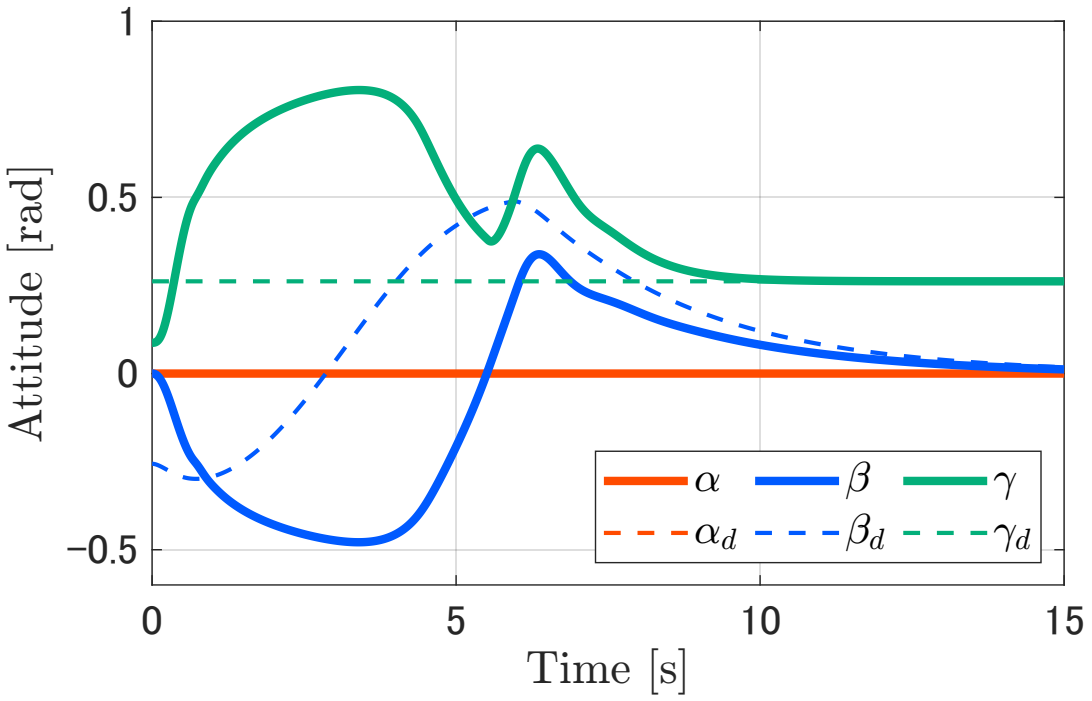

Figure 6. Simulation result of attitude.

References

[1] Kooijman D, Schoellig AP, Antunes DJ. Trajectory Tracking for Quadrotors with Attitude Control on $\mathcal{S}^2 \times \mathcal{S}^1$. In: 2019 18th European Control Conference (ECC); Jun.; Naples, Italy. IEEE; 2019. p. 4002–4009.

[2] Lee T, Leok M, McClamroch NH. Control of Complex Maneuvers for a Quadrotor UAV Using Geometric Methods on $SE(3)$; 2011.

[3] Lee T, Leok M, McClamroch NH. Geometric Tracking Control of a Quadrotor UAV on $SE(3)$. In: 49th IEEE Conference on Decision and Control (CDC); Dec.; Atlanta, GA. IEEE; 2010. p. 5420–5425.

[4] Fan DD, Thakker R, Bartlett T, et al. Autonomous Hybrid Ground/Aerial Mobility in Unknown Environments. In: 2019 IEEE/RSJ International Conference on Intelligent Robots and Systems (IROS); Nov.; Macau, China. IEEE; 2019. p. 3070–3077.

[5] Kalantari A, Spenko M. Design and experimental validation of HyTAQ, a Hybrid Terrestrial and Aerial Quadrotor. In: 2013 IEEE International Conference on Robotics and Automation; May; Karlsruhe, Germany. IEEE; 2013. p. 4445–4450.

[6] Wu T, Zhu Y, Zhang L, et al. Motion Planning for HyTAQs: A Topology-guided Unified NMPC Approach. In: 2022 IEEE/RSJ International Conference on Intelligent Robots and Systems (IROS); Oct.; Kyoto, Japan. IEEE; 2022. p. 4835–4840.

[7] W BR. Asymptotic Stability and Feedback Stabilization. Differential Geometric Control Theory. 1983;27:181–191. Available from: `https://cir.nii.ac.jp/crid/1572824499073211520`.

[8] Bhat SP, Bernstein DS. A Topological Obstruction to Continuous Global Stabilization of Rotational Motion and the Unwinding Phenomenon. Systems & Control Letters. 2000; 39(1):63–70. Available from: `https://www.sciencedirect.com/science/article/pii/S0167691199000900`.

[9] Rodríguez-Cortés H, Velasco-Villa M. A New Geometric Trajectory Tracking Controller for the Unicycle Mobile Robot. Systems & Control Letters. 2022 Oct;168:105360.

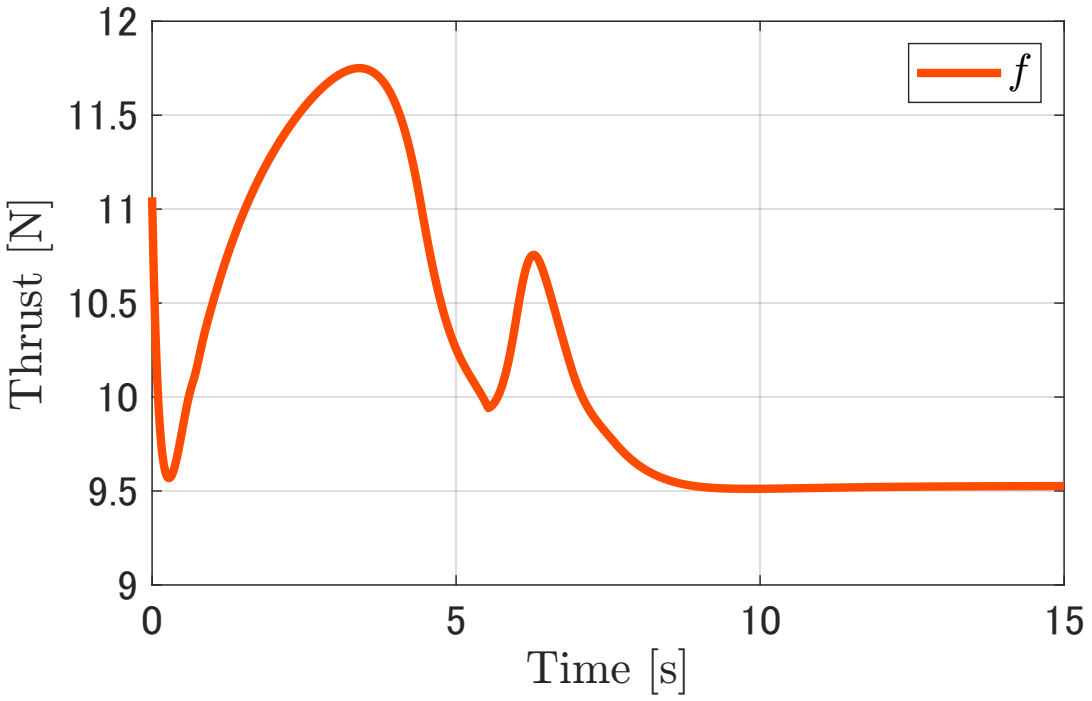

Figure 7. Simulation result of thrust.

[10] Lee T, Leok M, McClamroch NH. Nonlinear Robust Tracking Control of a Quadrotor UAV on $SE(3)$. Asian Journal of Control. 2013;15(2):391–408. Available from: `https://onlinelibrary.wiley.com/doi/abs/10.1002/asjc.567`.

[11] Angeli D. Almost Global Stabilization of the Inverted Pendulum via Continuous State Feedback. Automatica. 2001;37(7):1103–1108. Available from: `https://www.sciencedirect.com/science/article/pii/S0005109801000644`.

[12] Ames AD, Xu X, Grizzle JW, et al. Control Barrier Function Based Quadratic Programs for Safety Critical Systems. IEEE Transactions on Automatic Control. 2017 Aug; 62(8):3861–3876.

[13] Ames AD, Coogan S, Egerstedt M, et al. Control Barrier Functions: Theory and Applications. In: 2019 18th European Control Conference (ECC); Jun.; Naples, Italy. IEEE; 2019. p. 3420–3431.

[14] Huang Y, Yong SZ, Chen Y. Guaranteed Vehicle Safety Control Using Control-Dependent Barrier Functions. In: 2019 American Control Conference (ACC); Jul.; Philadelphia, PA, USA. IEEE; 2019. p. 983–988.

[15] Li B, Wen S, Yan Z, et al. A Survey on the Control Lyapunov Function and Control Barrier Function for Nonlinear-Affine Control Systems. IEEE/CAA Journal of Automatica Sinica. 2023 Mar;10(3):584–602.

[16] Ames AD, Grizzle JW, Tabuada P. Control Barrier Function Based Quadratic Programs with Application to Adaptive Cruise Control. In: 53rd IEEE Conference on Decision and Control; Dec.; Los Angeles, CA, USA. IEEE; 2014. p. 6271–6278.

[17] Xiao W, Belta C. Control Barrier Functions for Systems with High Relative Degree. In: 2019 IEEE 58th Conference on Decision and Control (CDC); Dec.; Nice, France. IEEE; 2019. p. 474–479.

[18] Desai M, Ghaffari A. CLF-CBF Based Quadratic Programs for Safe Motion Control of Nonholonomic Mobile Robots in Presence of Moving Obstacles. In: 2022 IEEE/ASME International Conference on Advanced Intelligent Mechatronics (AIM); Jul.; Sapporo, Japan. IEEE; 2022. p. 16–21.

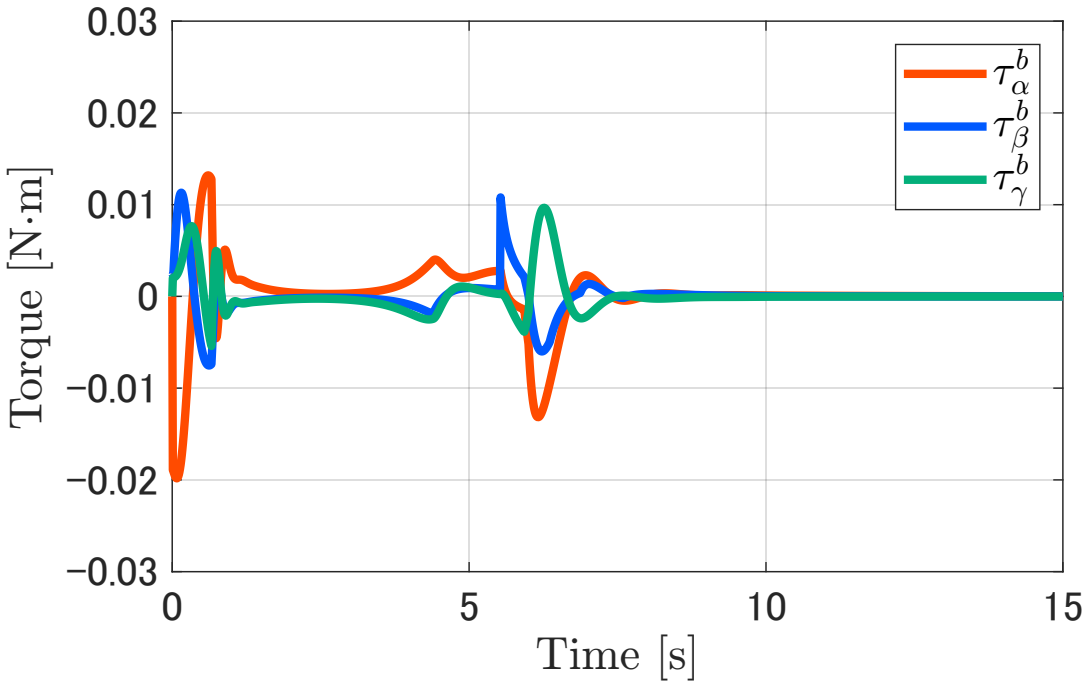

Figure 8. Simulation result of torque.

[19] Marley M, Skjetne R, Teel AR. Synergistic control barrier functions with application to obstacle avoidance for nonholonomic vehicles. In: 2021 American Control Conference (ACC); May; New Orleans, LA, USA. IEEE; 2021. p. 243–249.

[20] Khan M, Zafar M, Chatterjee A. Barrier Functions in Cascaded Controller: Safe Quadrotor Control. In: 2020 American Control Conference (ACC); Jul.; Denver, CO, USA. IEEE; 2020. p. 1737–1742.

[21] Wu G, Sreenath K. Safety-Critical Control of a Planar Quadrotor. In: 2016 American Control Conference (ACC); Jul.; Boston, MA, USA. IEEE; 2016. p. 2252–2258.

[22] Nonami K, Kendoul F, Suzuki S, et al., editors. Autonomous Flying Robots: Unmanned Aerial Vehicles and Micro Aerial Vehicles. Tokyo ; New York: Springer; 2010. OCLC: ocn471803402.

[23] Wu T, Zhu Y, Zhang L, et al. Unified Terrestrial/Aerial Motion Planning for HyTAQs via NMPC. IEEE Robotics and Automation Letters. 2023 Feb;8(2):1085–1092.

[24] Tayefi M, Geng Z. Logarithmic Control, Trajectory Tracking, and Formation for Nonholonomic Vehicles on Lie Group $SE(2)$. International Journal of Control. 2017 06;92.

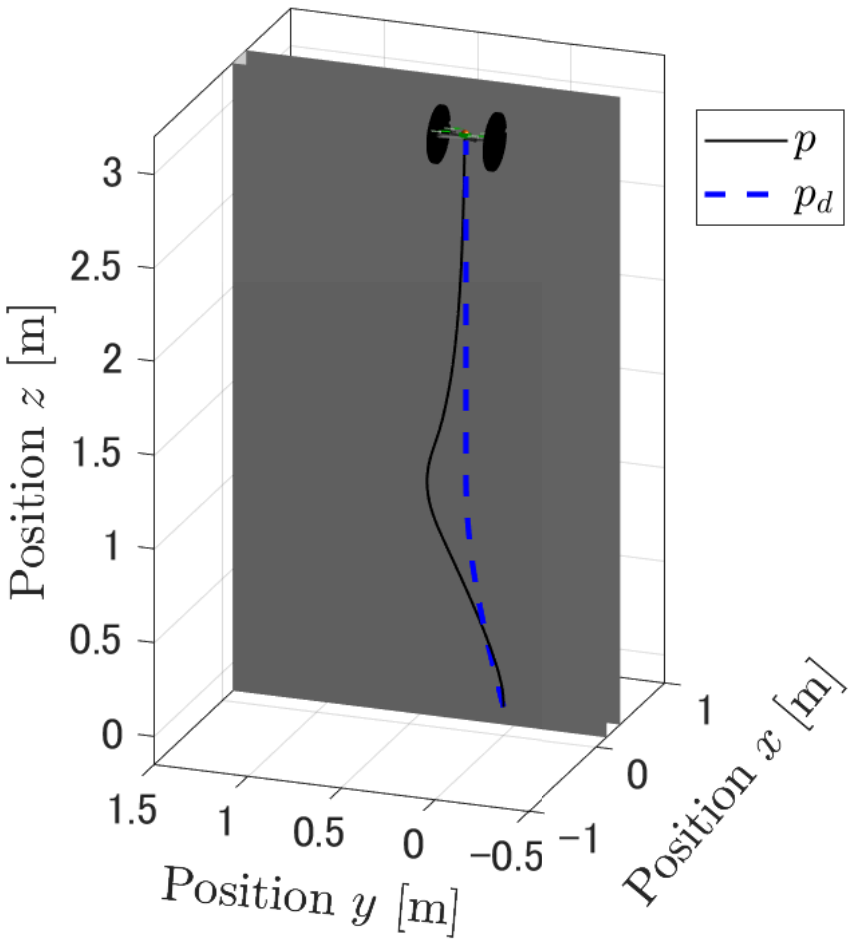

Figure 9. Animation of the simulation result.

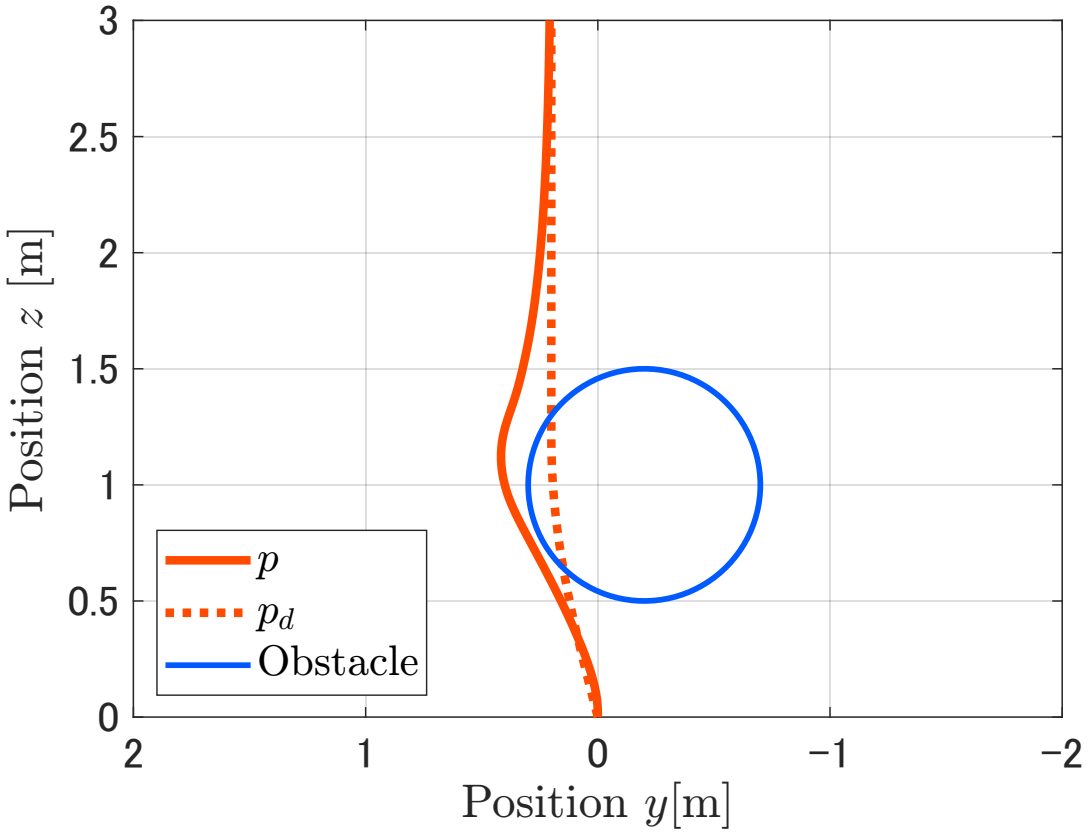

Figure 10. Trajectory of the simulation result.

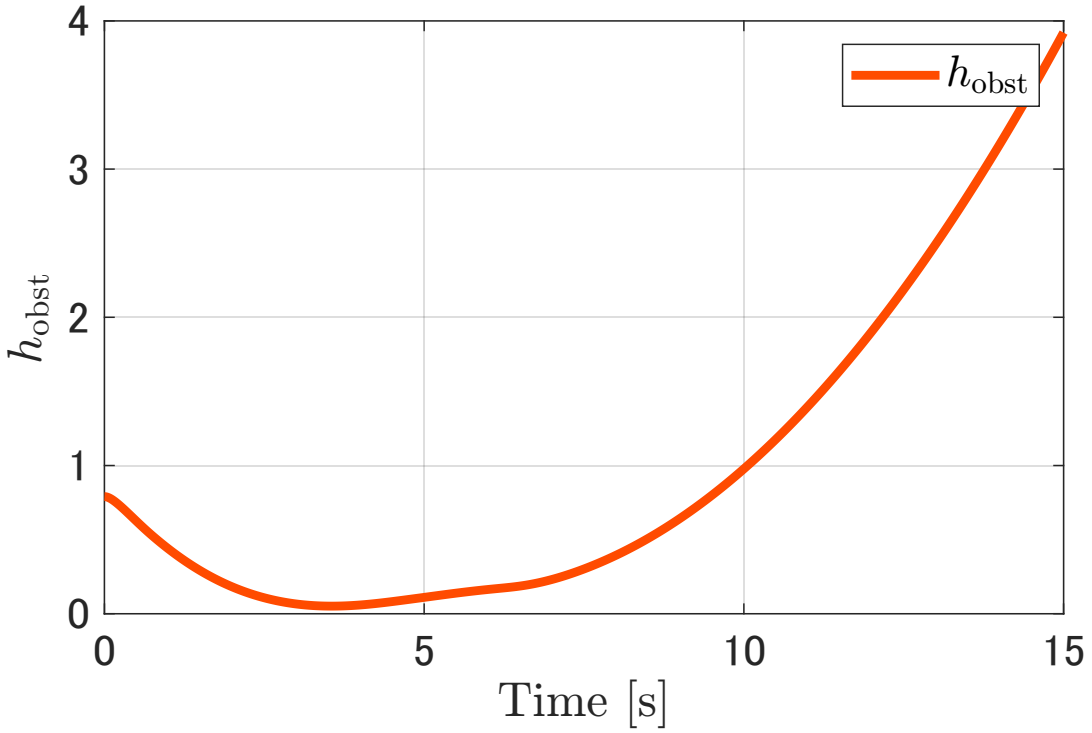

Figure 11. Obstacle CBF of the simulation result.

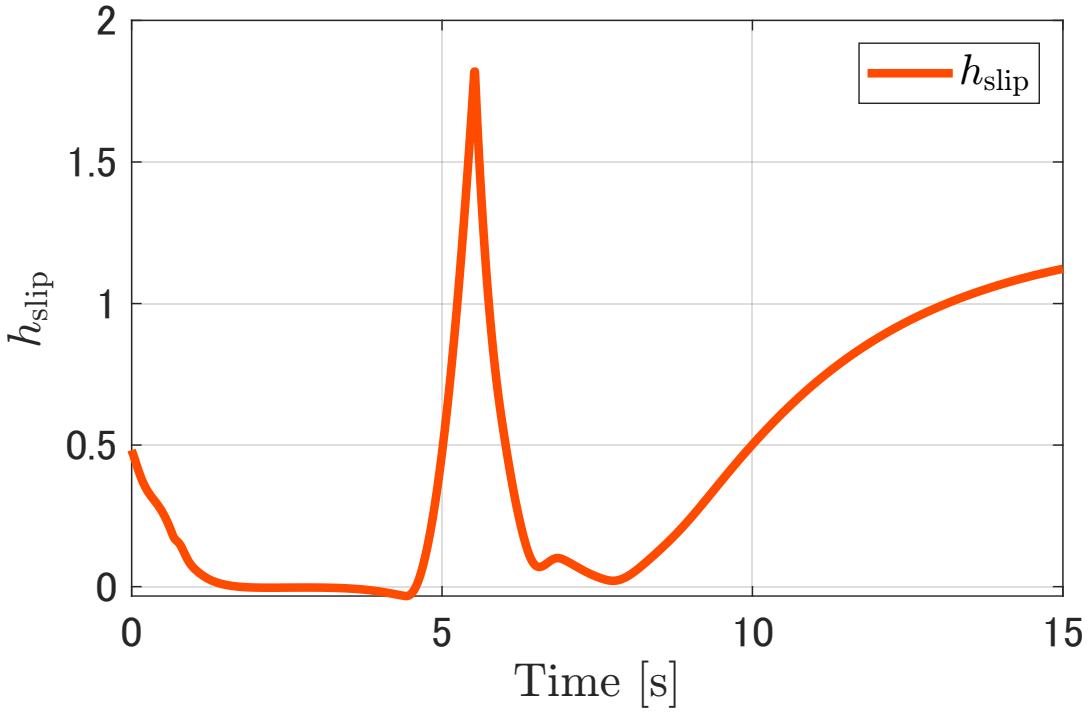

Figure 12. Sideslip CBF of the simulation result.